Electronic Notes in Theoretical Computer Science 46 (2001)
URL: http://www.elsevier.nl/locate/entcs/volume46.html 16 pages

Digital Projections in Prime and Composite Arrays

Imants Svalbe [1,2]

School of Physics and Materials Engineering
Monash University
Clayton, Australia

Abstract

The Discrete Radon Transform (DRT) provides a 1:1 mapping between any discrete array, for example a 3D micro-crystal or a 2D digital photograph, and its digital projections. The DRT is both conceptually simple and computationally efficient, yet has an engaging richness of descriptive power in characterising discrete systems. So far the DRT has been applied to the reconstruction and analysis of digital images based on digital projections, but it would appear that the DRT has much more to offer. The DRT has roots in fundamental number theory through pseudo-random sequences as well as the distribution of the number of primes and hence with the zeros of the Riemann zeta function. The linkage of these number-theoretic aspects to the properties of physical systems means the DRT may find application in diverse fields. It may be possible to model the chaotic behaviour of the energy spectra of discrete systems using a set of basis functions derived from the DRT. This paper describes the intrinsic properties of discrete arrays as defined by the sets of digital projections generated by the 2D DRT. In particular, it presents details of the angle and sampling distance interval distributions for digital projections, for square and hexagonal arrays of prime and composite size. Arrays of composite size are of interest in representing the spectral properties of crystals containing granular domains of variable size.

1 Introduction

The key ideas here rest on the fact that shape and content of any discrete or granular assembly of "atom-like" points, such as those found in a poly-atomic crystal or as pixels in a digital photograph, can be exactly described by a unique set of digital projections. The requisite theory for this description is

[1] Thanks to Assoc. Prof. Charles Osborne for helpful comments and to Steven Homolya from Monash University for assistance and suggestions with manuscript preparation.
[2] Email: imants.svalbe@spme.monash.edu.au

an extension of the continuous space Radon projective transformation [7] to the digital projections defined for objects comprised of sampled values located on discrete, regular lattice spaces.

1.1 The Discrete Radon Transform

The Radon transform [7] is based on the properties of integrals taken along straight lines through an object. The continuous space Radon projective transformation has an inversion formula that permits close approximation of the shape of an arbitrary object given a sufficiently representative set of discrete, sampled projections (for example, x-ray transmission profiles) of that object.

The Discrete Radon Transform (DRT) operates on arbitrary objects embedded in a discrete rather than continuous space. An image $I(x, y)$ maps to its DRT, $R(t, m)$, where I is a discrete object sampled at regular locations x and y, and R is a set of digital projections with translates t and angles m, with x, y, t and m integers. A general definition of the DRT was developed by Beylkin [1] for discrete rectangular arrays of arbitrary integer size. Beylkin developed an exact algebraic formalism for the discrete projection and inversion process, established a connection between the DRT and the discrete Fourier transform (both processes are 1:1 mappings of the original discrete set) and provided an efficient algorithm for its computation. Beylkin also included the possibility of the projections being taken along curved as well as straight paths. The addition of curved path projections is an essential extension when inverting projections from seismic imaging, where rays experience significant refraction, such as also occurs in ultrasound CT. Beylkin also foreshadowed the implementation of filtering and other spatial operations in 2D or higher spaces by computation of these properties in the DRT space. The Radon transform shares much in common with the Hough transform used to segment lines or shapes in digital images and the DRT is strongly related to discrete representations of straight lines used for a discretised version of the Hough Transform [9].

The definitions adopted here for digital projection mapping are those of Matus and Flusser [6], who outlined the group theoretic and Fourier interpretations of the DRT, as applied to 2D arrays of prime dimension. They described application of the DRT as a relatively efficient data compression mechanism for digital images. When the array size is restricted to be a prime rather than an arbitrary integer, the set of projections becomes non-degenerate, as each array point is sampled once and only once, in a pattern that is unique for each projection. The projection and inversion process then becomes a simple arithmetic (additive) operation rather than more general algebraic transformation of Beylkin's DRT scheme.

Salzberg [8] applied the DRT to image the structure of 3D crystals from their real x-ray transmission profiles and showed it was possible to invert real x-ray projection data using the DRT under an iterative reconstruction

formula. Svalbe [11] applied the DRT formalism to directly compute grey scale images from real space projection data and demonstrated the reconstruction conditions required to produce images of comparable quality to those obtained by using conventional CT methods. The DRT principles are also well known and applied in discrete tomography [3] and are used as a tool in mathematical lattice theory [5].

The concept that digital projections can represent exactly all of the information in discrete sets also offers immediate practical benefit in applications involving (or manipulating) discrete objects. For example, Svalbe [10] has shown that the DRT provides a suitable framework for the imperceptible orientation-sensitive embedding of messages or structural information in discrete images and provides an orientation-sensitive, non-linear model useful for the description of local textures.

The conservation of information between a digital image and its digital transformation also means that projections with the largest percentage of descriptive information can be selected and used to guide real space limited angle acquisition systems to achieve optimal image recovery from a limited number of views.

1.2 Number Theory and the DRT

Remarkably, the DRT has significant links with the famous "Riemann Hypothesis", concerning the distribution of zeros of the Riemann zeta function. The "Adeles" system of Connes, as presented in a recent review [4], is an n-dimensional, n-addic, imaginary space with energy levels that match the pattern formed by the density of prime numbers and hence the real ($s = \frac{1}{2}$) zeros of the Riemann zeta function.

The DRT formalism, applied to 2D discrete lattices, appears to constitute a practical, concrete example of an Adeles system because the distribution of (squared) gap distances is also based on a selected set of prime integers and hence is endowed with the same representational complexity.

As pointed out by Berry in [4], the mean energy distribution of an ensemble of quantum chaotic systems also matches the Riemann zeta zeros distribution. Number theorists Sarnak and Katz also reported in [4] that a spectral interpretation can be applied to not only the zeros of the Riemann zeta function, but also to many other zeta-like number-theoretic functions.

The DRT formalism links quantum chaos and real discrete systems by relating the behaviour of excitations, propagating (like digital projections) along lines between array-selected nearest neighbours, to the spectral distribution of energy states for real discrete objects. The (unique) distribution of minimal gap distances between the digital samples may serve as a basis to describe the spectrum of the energy of individual electrons (or other wave excitations such as phonons) propagating along discrete straight line trajectories within objects composed of discrete elements, just as the spacing of atomic planes

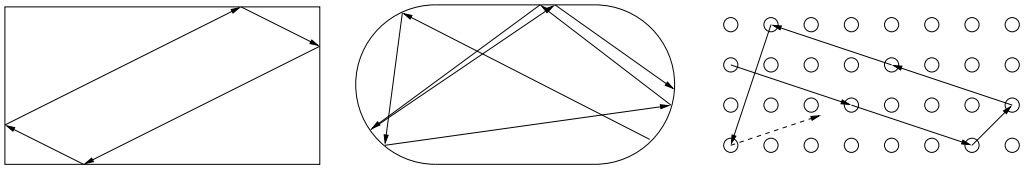

(a) (b) (c)

Fig. 1. Examples of excitation trajectories in finite systems: a) deterministic paths in classical regular objects, b) classical chaotic paths in the "stadium billiards" case, and c) chaotic / quantum trajectories for excitations in finite, discrete systems

defines the Bragg reflections in x-ray diffraction.

The path-lengths (and hence wavelengths) of excitations propagating along arbitrary trajectories that are constrained to lie within compact (but continuous) 2D or 3D boundaries may be simply periodic for rectangular objects as shown in Fig. 1a, or chaotic [2], for the "stadium billiards" case (a rectangle with curved ends), as shown in Fig. 1b. Quantum chaos solutions are often required to describe the complex energy states of finite, discrete objects such as that shown in Fig. 1c.

For discrete objects, the underlying lattice provides potential wells that constrain the paths of excitations away from trajectories at arbitrary orientations and biases them towards orientations supported by links to nearest "atomic" neighbours. The energies of these states will be inversely proportional to the length, or the squared length, of the minimal paths defining these trajectories. The connection between classical chaotic orbits and quantum eigenvalues (as "trace formulae") was made, forty years ago, by Gutzwiller [2].

Discrete objects could be modelled as being embedded in a regular array of next-largest prime size. To enable optimal matching of the object properties to the properties of the array, arrays are selected with, as near as possible, the same size and real space symmetry as the object. These requirements motivated this examination of the properties of the DRT on square and hexagonal lattices. Arrays of composite size are also examined to enable a more general sizing approach for arbitrary shaped and relatively disconnected objects, for example, as a complex array built or tiled from an assembly of loosely coupled prime sub-arrays. The DRT formalism can also define objects of arbitrary shape on a lattice of size equal to the bounding square and then using a site-occupancy variable as one of the discrete array function values.

Another number-theoretic connection is the occurrence of primitive root or Legendre sequence generators within the DRT. When mapped as phase vectors on the unit circle, the Legendre sequences have the interesting property that they are invariant under Fourier transformation [13]. Related sequences occur, for example, in the generation of a cyclic mapping on the rows and columns in $R(t, m)$ space so that the reconstructed image is rotated by 90° [12]. The rotational mapping sequences in this case are of prime length p and are based

on p and the integer quotients $(p-1+\alpha_i p)/i$ for $1 \leq i \leq p-1$ and integers $\alpha_i \geq 0$.

1.3 Structure of this Paper

The DRT formalism and its relationship to image reconstruction is defined for a square array in section 2, followed by a brief description of the extension of the DRT to hexagonal arrays in section 3. Section 4 presents an overview of the systematic behaviour of the angle and the gap distance distributions for digital projections on arrays of prime size. Where possible, equations have been given to link the DRT variables, otherwise tables or illustrative figures are used to demonstrate consistent trends observed over the large range of array sizes examined. Section 4.3 presents the changes observed in these distributions for arrays of composite rather than prime size. Section 5 provides some conclusions.

2 The DRT Formalism

The DRT maps, exactly and invertibly, between any discrete set and its set of suitably defined projections. The digital projections provide an insightful description of the original object couched in terms of a unique set of discrete projection angles, with parallel samples taken at uniformly spaced (integer) translations. The sampling of object values within the object "body", along the direction of the digital projection rays, also occurs at discrete intervals (as opposed to the continuous integral sampling of the original Radon transform). This discrete "gap" distance, the interval between successive digital samples along a digital ray, is discussed in detail in section 4.

The DRT properties are illustrated here by a 2D example (for higher dimensions, the 2D plane can be mapped to a torus [8]). The conventional DRT works on prime p sized arrays and was developed to project the discrete elements (pixels) of digital images. When considering real, discrete atomic systems rather than digital images, the value at each array site may be interpreted in several (multispectral) ways; as some numeric property of the array at that point (for example, the local electron density), or as a (constant) label to denote the type of atomic species at each site, or as a binary value (for filled/vacant lattice sites).

The DRT maps a 2D $p \times p$ digital image, $I(x, y)$, to a 2D $p \times (p+1)$ digital space, $R(t, m)$, comprised of "1D" digital projections. The coordinates x, y, t and m are all integers. The origin $(0, 0)$ of each space is (arbitrarily) taken to be the element in top left corner of the array. Each digital projection has p uniform translates (here called projection "rays"), labelled by an index, t, $(0 \leq t < p)$ and each projection occurs at one of $p+1$ digital "angles", indexed by m $(0 \leq m \leq p)$.

Fig. 2 shows the links between a real object O, its discrete analog projec-

$$\begin{array}{lcl} \text{Digital Image} & I(x,y) \Longleftrightarrow R(t,m) & \text{Digital Projection} \\ & \Downarrow\uparrow \quad \nwarrow \quad \Downarrow\uparrow & \\ \text{Object} & O \implies P(\rho,\theta) & \text{Analog Projections} \\ & & (\rho \text{ sampled at } \theta \text{ angles}) \end{array}$$

Fig. 2. The connections between a real object, its image and projection.

$I(x,y)$	$x=0$	$x=1$	$x=2$
$y=0$	**1**	**2**	**3**
$y=1$	**4**	**5**	**6**
$y=2$	**7**	**8**	**9**

Table 1
A sample digital 3×3 image, $I(x,y)$.

tion P, the digital image I, and the digital projection R, of the same object. The link between I and R is exactly 1:1 and invertible, so that information about the image I (such as the total variance) is distributed (usually non-uniformly) across R, the set of digital projections. O is not unique for any given set of discrete projections P, but P can be made sufficiently representative to make I a close approximation of O. It is possible to map exactly from R to P but mapping from P to R is, like mapping from P to I or from O to I, a lossy process that depends on the details of the continuous to discrete mapping.

To generate a single digital projection, (t,m), the image pixel value at translate $x=t$, $y=0$, is summed with the pixel value at $x=(t+m) \bmod(p)$, $y=1$, then at $x=(t+2m) \bmod(p)$ on $y=2$ and so on, up to and including $y=p-1$. The projections are generated by repeating this process for all possible values of t and m. The digital projection $m=p$ is an exception, with summations for each t being taken across one of the p rows. This process is illustrated by the data in Table 1, for a 3×3 discrete, square lattice array, with sites labelled from 1 to 9. Table 1 may equally well be regarded as a greyscale digital image, $I(x,y)$ with 9 arbitrarily valued levels or shades of grey. Table 2 shows the DRT of the data in Table 1.

Because the array is of prime size, each pixel is selected, for any choice of t and m, just once from a unique pattern of locations, and hence the projections are exactly invertible. The inverse DRT writes back each of the $R(t,m)$ values across the image space $I(x,y)$ in the same spatial pattern as they were obtained. The reconstruction (back-projection) process is almost identical to

$R(t,m)$	$t=0$	$t=1$	$t=2$
$m=0$	$\mathbf{1,4,7}$	$\mathbf{2,5,8}$	$\mathbf{3,6,9}$
$m=1$	$\mathbf{1,5,9}$	$\mathbf{2,6,7}$	$\mathbf{3,4,8}$
$m=2$	$\mathbf{1,6,8}$	$\mathbf{2,4,9}$	$\mathbf{3,5,7}$
$m=3$	$\mathbf{1,2,3}$	$\mathbf{4,5,6}$	$\mathbf{7,8,9}$

Table 2
The DRT, $R(t,m)$, of image $I(x,y)$ of Table 1.

$I'(x,y)$	$x=0$	$x=1$	$x=2$
$y=0$	$\mathbf{1,2,3}$ $\mathbf{1,5,9}$ $\mathbf{1,6,8}$ $\mathbf{1,4,7}$	$\mathbf{1,2,3}$ $\mathbf{2,6,7}$ $\mathbf{2,4,9}$ $\mathbf{2,5,8}$	$\mathbf{1,2,3}$ $\mathbf{3,4,8}$ $\mathbf{3,5,7}$ $\mathbf{3,6,9}$
$y=1$	$\mathbf{4,5,6}$ $\mathbf{3,4,8}$ $\mathbf{2,4,9}$ $\mathbf{1,4,7}$	$\mathbf{4,5,6}$ $\mathbf{1,5,9}$ $\mathbf{3,5,7}$ $\mathbf{2,5,8}$	$\mathbf{4,5,6}$ $\mathbf{2,6,7}$ $\mathbf{1,6,8}$ $\mathbf{3,6,9}$
$y=2$	$\mathbf{7,8,9}$ $\mathbf{2,6,7}$ $\mathbf{3,5,7}$ $\mathbf{1,4,7}$	$\mathbf{7,8,9}$ $\mathbf{3,4,8}$ $\mathbf{1,6,8}$ $\mathbf{2,5,8}$	$\mathbf{7,8,9}$ $\mathbf{1,5,9}$ $\mathbf{2,4,9}$ $\mathbf{3,6,9}$

Table 3
Image $I(x,y)$ reconstructed from the digital projection data $R(t,m)$ of Table 2.

that for forward projection, rather like the Fourier transform. When the DRT forward mapping is applied twice, the resulting image is a reflected image of the original (again $m = p$ requires special processing [12]).

The DRT projection and inversion algorithms are true backprojection methods and so require access to all $p \times p$ pixels for all $p+1$ values of m, i.e. $O(p^3)$. The only operation required for each data point accessed is addition. Faster and more efficient algorithms exist for inverting projections (see the text by Herman and Kuba in [8]) but these involve multiplication of the original data values.

Table 3 shows the reconstructed image values obtained from Table 2 via the inverse DRT. Note each reconstructed pixel contains p times the original value at that image location, plus a value equal to the summed intensity of the whole image. Like the Fourier transform, the DRT mapping is 1:1; after normalisation, the reconstructed image is identical to the original, so the projection process is lossless.

The digital rays for each m value form characteristic projection angles in a manner reminiscent of the analogue projection case. The digital angles are given by $\theta_m = \arctan(x_m/y_m)$, where x_m and y_m are the Cartesian components of the nearest-neighbour distances between pixels along the direction of a

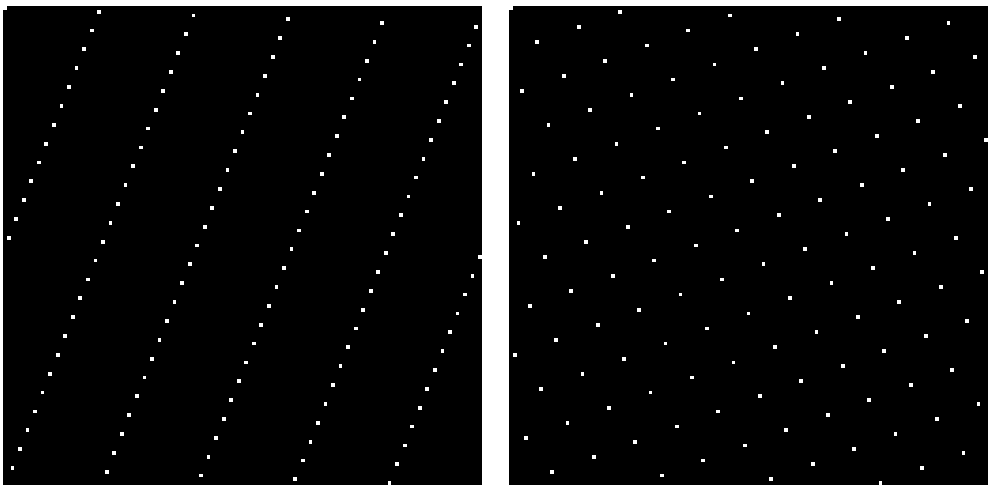

(a) (b)

Fig. 3. Digital rays for $p = 127$, $t = 0$, a) $m = 25$, $x_m = -2$, $y_m = 5$, $\theta_m = 158°$, b) $m = 29$, $x_m = 7$, $y_m = 9$, $\theta_m = 38°$.

common digital ray. A zero angle here is defined in the downwards vertical direction, 90° corresponds to the right horizontal axis direction. Digital rays form as (m, m') pairs oriented at complementary angles $\theta_{m'} = 180° - \theta_m$, where $\theta_{m'} = \arctan(-x_m/y_m)$ and $m+m' = p$ [11]. Unlike the analogue case, a single digital projection ray for a given translate, t, may wrap several times around the array, creating a bundle of rays with a common, parallel orientation.

This is shown in Fig. 3a for the case $p = 127$, for a square lattice, with $t = 0$ and $m = 25$. In Fig. 3a, the gap distance between sample along the ray direction ($d_{25}^2 = 29$) is relatively small in comparison to the distance between the wrapped sections, leading to well defined digital rays.

A given (squared) gap distance d_m^2 on a square array will always be an integer (x_m and y_m are respectively integer horizontal and vertical displacements on a lattice) and corresponds to values given by the minimal solution of a Diophantine equation

$$d_m^2 = x_m^2 + y_m^2, \tag{1}$$

where the range of solutions to search over is $0 \le x_m \le d_m$ and $1 \le y_m \le d_m$ and m is given by

$$m = \frac{\alpha p + x_m}{y_m}, \tag{2}$$

with α a positive integer such that m is an integer less than p. Fig. 3b shows the diffuse pattern of digital rays for the $p = 127$ array at $m = 29$; despite the large nearest-neighbour spacing ($d_{29}^2 = 130$) a unique set of colinear sample points is still evident.

For an array with square symmetry, the primes p can be expressed as two types, $4n + 1$ and $4n + 3$. This distinction will become important in characterising the distribution of d_m^2 values. The four-fold symmetry allows the

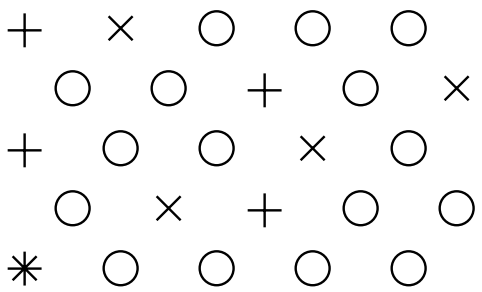

Fig. 4. Example of a digital projection on a hexagonal array. The elements marked $\otimes$ form the projection $t = 1$, $m = 3$ with $p = 5$, those marked $\oplus$ form $t = 0$, $m = 2$ (the [[?]] marks an intersection of the two projections).

solutions $\pm x_m : y_m$ and $\pm y_m : x_m$, forming two sets of complementary angle pairs, with each of these four projections having the same value of d_m^2. An exception occurs at angles $0°$ and $90°$ (where $d^2 = 1$ with $m = 0$ and $m' = p$ respectively) and at $45°$ and $135°$ (where $d^2 = 2$ with $m = 1$ and $m' = p - 1$ respectively) as these projections form single pairs of digital rays at complementary angles. The $4n + 3$ primes form $4n$ angles (excluding $0°, 45°, 90°$ and $135°$) and hence show exact four-fold symmetry. The $4n+1$ primes form four-fold symmetric angles except at two m values where two pairs of equivalent angles are formed, each with $d_m^2 = p$.

3 The DRT on Hexagonal Arrays

We define a square array built from a hexagonal lattice as shown in Fig. 4. The translations in the horizontal translate (t) direction have unit spacing, as for the square lattice. Adjacent rows in the vertical direction are now separated by a distance of $\sqrt{3}/2$ and are offset horizontally by 0.5 unit spacing. We define a digital projection (t, m) to start with the content of the discrete array found at translate t (with the origin at the left of the top row as before) and sum this with the content at $\left((t + m) \bmod(p) + \frac{1}{2}, 1\right)$ and continue the summation until row $p-1$ has been processed. An alternative method to form the digital projections would be to snap back to the array point $\left((t + m) \bmod(p) - \frac{1}{2}, 1\right)$ and to reverse the indentation of rows; adopting this definition simply reduces the effective value of m to $m - 1$.

The zero angle is here defined again as the direction of the downward vertical axis. The projection $m = 0$ is taken across the rows to form the $90°$ projection, because now $m = (p - 1)/2$ selects pairs of even and odd offset columns of the hexagonal array and so forms the zero degree projection. For $m = 1$ the projections are always at $60°$. For $m = p$, the angle is always $30°$, similarly $m = p - 1$ will always form digital rays at $150°$ and $p - 2$ is always oriented at $120°$. Projection m has a complementary projection at $m' = p - 1 - m$, with $\theta_m + \theta_{m'} = 180°$.

Because the horizontal distances accrue in 0.5 units (even though the array

translates for t and m are integer increments), it is useful to define, for hexagonal arrays, the relative displacement x_m as integer multiples of 0.5 units. A given (squared) gap distance d_m^2 on a hexagonal array will then, as for the square array, always turn out to be an integer (x_m and y_m are respectively integer horizontal and vertical displacements on a lattice). As array points are separated by multiples of 0.5 units horizontally and $\sqrt{3}/2$ units vertically, the distance between lattice points along the digital ray directions is given by the minimal solutions of the Diophantine equation

$$4d_m^2 = x_m^2 + 3y_m^2, \tag{3}$$

where the range of solutions to search over is $0 \leq x_m \leq \text{int}(2d_m)$ and $0 \leq y_m \leq \text{int}(2d_m/\sqrt{3})$, where int() is the function returning the integer part of its argument, and m is given by

$$m = \frac{\left[\alpha p + \frac{1}{2}(x_m - y_m)\right]}{y_m}, \tag{4}$$

with α a positive integer such that m is an integer less than p. Here x_m and y_m must be both even or both odd (or the displacements fall between lattice locations). The squared distance between adjacent pixels along these digital rays on a hexagonal lattice is then always an integer (as for the square lattice), as $x_m^2 + 3y_m^2$ will always be a multiple of 4 when x_m and y_m are both even or are both odd.

Primes on a hexagonal array can be of two types, $6n+1$ or $6n+5$, with n a positive integer. The $6n+1$ primes generate $6n+2$ angles in $R(t, m)$, forming as $3n + 1$ angle and complementary angle pairs. The $6n + 2$ corresponding values of d_m^2 are grouped in multiples of six, because 3 pairs of rays, each separated by relative angle increments of 60° and having the same sampling interval, form on hexagonal sites. This leaves one pair of m values which have the maximum value of $d_m^2 = p$. The m values corresponding to the largest value of distance also have three equivalent angles, spaced 60° apart, any one of which may be assigned as the angle for that m. The $6n + 5$ primes form $6n + 6$ angles as complementary pairs with each group of six angles sharing the same distance value.

4 Distribution of Angles and Distances

4.1 The Prime Square Array

The angle distribution is generated by evaluating and selecting the minimum value of d between the sample pixels for all possible (coprime) solutions x_m, y_m of (1) for each value of m, at some fixed prime value for p. It shows no degeneracy for prime p, so each digital projection angle is unique [11]. Of interest here is the distribution of squared minimal gap distances between pixel samples along the ray directions ($d_m^2 = x_m^2 + y_m^2$). For a square lattice, the maximum value of d_m^2 varies quite erratically as a function of p, but converges to around $1.14p$ for p large [11]. The (ranked) angle and gap distributions are

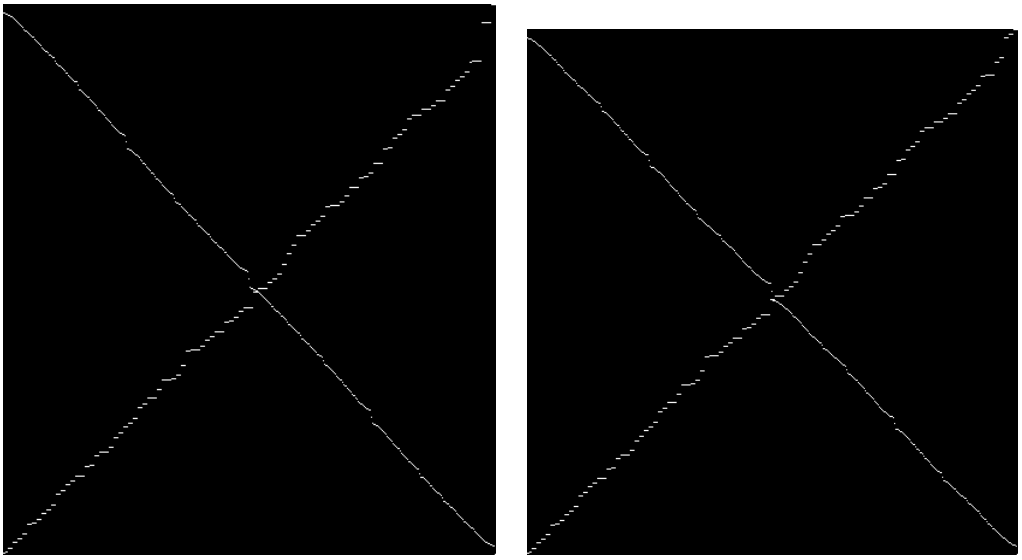

(a) (b)

Fig. 5. Distribution of the $p+1$ sorted angles, left axis $180° > \theta \geq 0°$, and the $p+1$ squared gap distances as a function of m for a square lattice of size $p \times p$ for a) $p = 409$, a $4n+1$ prime, right axis $1 \leq d^2 \leq 457$, and b) $p = 419$, a $4n+3$ prime, right axis $1 \leq d^2 \leq 449$.

shown for a square lattice in Fig. 5a for $p = 4n+1$ and Fig. 5b for $4n+3$. The angle distribution shown in the following figures runs from top left ($\theta = 180°$) to bottom right ($\theta = 0°$); the gap distribution runs from bottom left ($d^2 = 1$) to top right (where $d^2 = 457$ in Fig. 5a, and $d^2 = 449$ in Fig. 5b). Both distributions are shown as a function of the $p+1$ values of m.

For a square lattice, the selected (or allowed quantised) values of the squared distances for $p = 4n+1$ and $4n+3$ is formed from the set of values given by

$$d^2 = \{1, 2, \text{ all } 4n+1 \text{ primes}\} \tag{5}$$

plus cross products of these terms up to the maximum value of $d^2 \approx 1.14p$.

Equation (1) permits integer solutions for d^2 of type $4n+1$ when d^2 is odd, and $2(4n+1)$ when d^2 is even. When x_m and y_m are coprime, the solutions are restricted to the set given by equation (5). The frequency, f, with which d^2 values occur is 2 for $d^2 < 5$ (and for the case $d^2 = p$, when p is a $4n+1$ prime). For other allowed values of d^2,

$$f(d^2) = 2 \cdot 2^{\phi}, \tag{6}$$

where ϕ is the number of distinct prime factors of d^2, for $d^2 \geq 5$. The d^2 distributions for different values of p are identical from $d^2 = 1$ up to some cutoff point (for example, up to $d^2 = 401$ for $p = 409$ and 419). When d^2 is close to its maximum value, f may have a value between 2^n and 2^{n+1}, such as 12. For larger values of p, where $d^2 < d^2_{\max}$, equation (6) is correct. At $d^2_m \simeq d^2_{\max}$, all allowed $x_m : y_m$ combinations may not fit into the $p+1$ values

of m.

4.2 The Prime Hexagonal Array

The maximum value of d^2 on a hexagonal array of prime size p is always $\leq p$ and equals p when $p = 6n + 1$. The $6n + 1$ primes have one pair of hexagonally symmetric projections at this largest gap distance. The distance between adjacent pixel samples along the ray direction is then the same as the distance between the (wrapped) parallel rays formed by the same translate value t. The set of sample points defined by each of the two m values with $d^2 = p$ can be described by digital rays at one of 3 hexagonally equivalent angles. For a $6n + 1$ prime array, these distances form regular hexagons with sides $d^2 = p$. We observe that, for $p = 6n + 1$, $m^2 = m' + \alpha p$ (α integer ≥ 0) when $d^2 = p$.

The angle distributions here are also generated by evaluating the minimum value of d for all possible solutions x_m, y_m, of equation (3) for each value of m, at some fixed prime value for p. Solutions x_m and y_m are coprime (bar the factor of 2 for even x_m and y_m pairs). The angle and distance distributions for the hexagonal array cases are shown in Fig. 6. These distributions also show no degeneracy; each digital projection angle is unique if p is prime.

The distribution of the minimal squared distances also turns out, as for the square array, to be very number selective. For example, $d^2 = 19$ (a $6n+1$ prime) and $d^2 = 3 \times 7 = 21$ are allowed values. For a hexagonal lattice, the selected (or allowed quantised) values of the squared distances for $p = 6n + 1$ and $p = 6n + 5$ is formed from the set of values given by

$$d^2 = \{1, 3, \text{ all } 6n + 1 \text{ primes}\} \tag{7}$$

plus cross products of these terms up to the maximum value for d^2 ($= p$ when $p = 6n + 1$). The frequency, f, with which these d^2 values occur is 2 for the case $d^2 = p$, when p is a $6n+1$ prime, and is 3 for $d^2 < 7$. For all other cases

$$f(d^2) = 3 \cdot 2^{\phi}, \tag{8}$$

where ϕ is the number of distinct prime factors of $d^2 \geq 7$. The d^2 distributions for different values of p are, as for the square arrays, identical from $d^2 = 1$ up to some cutoff point (for example, up to $d^2 = 361$ for $p = 409$ and 419).

4.3 Distributions for Arrays of Composite Size

Fig. 7 shows the distributions of angles and minimal distances for a conventional DRT applied to an array, not of prime size, but of composite side length, $p = 408 = 2^3 \times 3^1 \times 17^1$. As might be expected, the set of minimally spaced digital projection angles is no longer unique, with some angles showing a high level of redundancy, especially at 0°(8), 30°(32) and 60°(12). For the square array, the redundancy is high at 0°(32), 45°(16) and 135°(16) (Fig. 7a). For the hexagonal array (Fig. 7b) at 30°, 16 of the 32 digital rays have $x_m : y_m = \pm 17 : 17$.

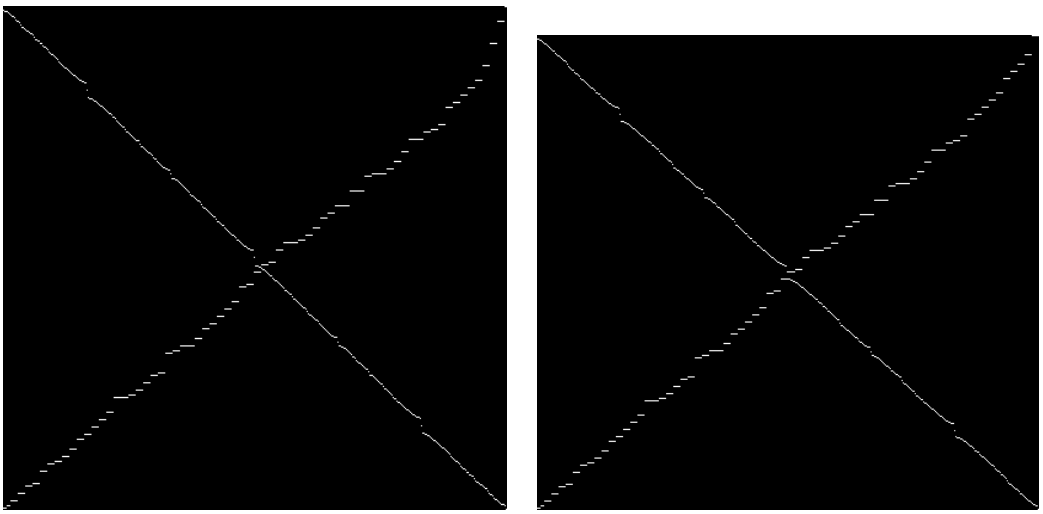

(a) (b)

Fig. 6. Distribution of the $p+1$ sorted angles, left axis $180° > \theta \geq 0°$, and the $p+1$ squared gap distances as a function of m for a hexagonal lattice of size $p \times p$ for a) $p = 409$, a $6n+1$ prime, right axis $1 \leq d^2 \leq 409$, and b) $p = 419$, a $6n+5$ prime, right axis $1 \leq d^2 \leq 397$.

The distribution of d^2 is correspondingly distorted (as each digital angle, m, has an associated minimal distance). Values of $6n+1$ primes are still selected in the hexagonal array case, but so too are new products (for example, $d^2 = 3 \times 4 = 12$ is now also allowed). These extra values of d^2 are generated by the term of j^2 which is added to the set of factors listed in equation (7), where j is a factor of the (now composite) value of p. With extra values of d^2 permitted, some of the prime array projections are displaced by the new composite array projections. Then $f(d^2)$ becomes 2ϕ, with ϕ being large, where d^2 has a large number of factors (for example $d^2 = 192 = 3 \times 4 \times 4 \times 4$ has $f = 16$). For the d^2 distribution on a composite sized square array, the situation is slightly more complex, as some multiples of the $4n+1$ prime values are completely suppressed by the insertion of the new j^2 terms.

4.4 Distributions at Fixed d^2 Values in Composite Size Arrays

If we fix on a selected value of d^2, we can look at how often that value is selected as a general function of the array size. This is equivalent to looking for prominent peaks in the energy spectra of crystalline systems with variable grain sizes. The frequency with which a given d^2 value occurs, with varying p, is periodic and the pattern of periodicity can be predicted, as can the m values that are associated with that d^2. The pattern of degeneracy can be complex, with long cycles of periodicity that are of interest in their own right. On hexagonal arrays, for the particular case $|x_m| = |y_m| = j$, then from (3) $d^2 = j^2$, so d is an integer. These rays correspond to digital projections at $\pm 30°$ or $\pm 150°$. The periodicity of the frequency distribution for hexagonal

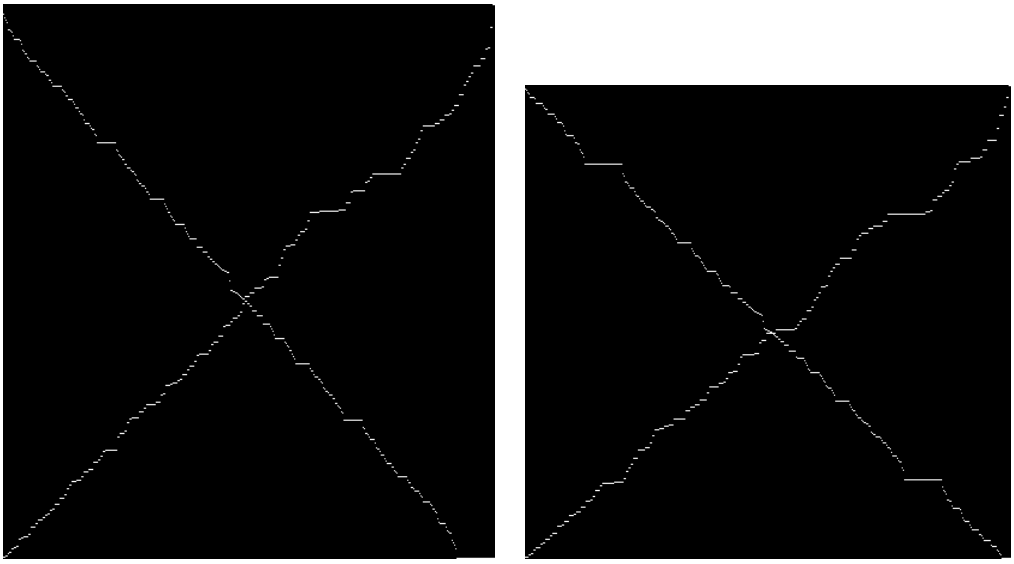

(a) (b)

Fig. 7. Distribution of the $p+1$ sorted angles, left axis $180° > \theta \geq 0°$, and the $p+1$ squared gap distances as a function of m for lattices of composite size $p \times p$ for $p = 408$. a) square lattice, right axis $1 \leq d^2 \leq 461$, b) hexagonal lattice, right axis $1 \leq d^2 \leq 397$.

arrays is particularly long when $d^2 = (6n+1)^2$. For example, $f(49)$ repeats after every 210 increments of p. For $d^2 = j^2$, $j \neq 6n+1$ prime, $f(d^2)$ is zero, except for every j^{th} entry, where $f = 4\phi$ for integer ϕ. The non-zero entries occur at composite array sizes p that are an integer multiple of j.

These results can be generalised to predict the distribution of minimal distances for arbitrary array sizes using equations (1) and (2) for the square arrays and (3) and (4) for the hexagonal arrays. The hexagonal cases are simpler to resolve because of the tighter upper bound on d^2.

The y_m values, as denominators in (2) and (4), produce cycles of length $\text{mod}(y_m)$ in the terms that contribute to each d^2 value. For example, the hexagonal solutions for $d^2 = 19$ have $y_m = 2, 3$ and 5, so that the net periodicity of $f(19)$ as a function of p is $2 \times 3 \times 5 = 30$. For $p = 408$, the 32 values of m contributing to $d^2 = 289 = 17^2$ include 16 degenerate pairs of m values, corresponding to $x_m : y_m = \pm 17 : 17$. These are generated because 17 is a prime factor of 408.

For composite hexagonal arrays of size p, the digital rays for $+j : j$ (30°) have m values given by $m = \alpha p/j$, and $-j : j$ (150°, the complementary angle) have m given as $\alpha p/j - 1$. This occurs because the nearest neighbour pixels must have horizontal offsets of $j/2$ after j row increments. Then $j(m+1/2) = p + j/2$, in agreement with (4).

The angle and distance distributions for composite arrays then turn out to be not too different from those for prime arrays. It is significant that arbitrary integers as large as 10^6 can be represented using only (on average)

(a) (b)

Fig. 8. a) original image "Lena", size 408×408, b) image reconstructed additively from a composite additive radon projection. The effects of redundancy in m at $0°$ and $45°$ cause the vertical and diagonal striping.

around 2.8 prime factors, each with a mean power of around 1.3. Composite arrays retain a large fraction of the prime-array exact representation properties and so may themselves adequately model many of the properties of discrete atomic systems, even without recourse to finding the algebraic solutions of [1]. Equivalently, the factorisation of a composite array into a small number of (sub-multiple) prime arrays will not become too complex so as to loose its descriptive utility. As a practical example, Fig. 8 shows that image data of composite size (408×408) appears quite recognisable, even after using the prime array formalism to project and reconstruct the image.

Equations (6) and (8) predict a large degeneracy in projections with d^2 comprised of many prime factors. For example, $d^2 = 32,045$ with factors 5, 13, 17 and 19 (the first four $4n + 1$ primes), produces $f = 32$. An equivalent observation is that a circle with a radius of this d will have, via equation (1), 64 square lattice points situated exactly on the circle perimeter.

5 Summary

The DRT on prime sized arrays has many interesting intrinsic properties because the prime integer and modulus operations interact to produce unique nearest-pixel angle distributions and very selective nearest-pixel distance distributions. The angle and distance distributions have been characterised for square arrays and the hexagonal array case, where the extra symmetry simplifies their interpretation considerably. We have characterised arrays of composite size to quantify the effects of degeneracy in projection angle and distance distributions. The work is motivated by applications in image reconstruction

and image encoding as well as using the DRT to study particle or excitation trajectories on regular lattices within real discrete "crystalline" systems.

References

[1] Beylkin, G., *Discrete Radon Transform*, IEEE Transactions on Acoustics, Speech and Signal Processing **35**(2) (1987), 162 - 172.

[2] Cipra, Barry, *A Prime Case of Chaos*, What is Happening in the Mathematical Sciences **4**, on-line article at `http://www.ams.org/new-in-math/cover/prime-chaos.html`.

[3] Correa, A., R. Cruz and P. Salzberg, *On a Spatial Limited Angle Model for X-ray Computerised Tomography*, Lectures in Applied Mathematics **30** (1994), 24-33.

[4] Klarrich, E., *Prime Time*, New Scientist **168**(No. 2264) (2000), 32 -36.

[5] Kung, J., *Radon Transforms in Combinatorics and Lattice Theory*, Contemporary Mathematics **57** (1986), 33-74.

[6] Matus, F., and J. Flusser, *Image Representations via a Finite Radon Transform*, IEEE T-PAMI **15**(10) (1993), 996-1006.

[7] Radon, J., *Uber die Bestimmung von Funktionen durch ihre Integralwerte langs gewisser Mannigfaltigkeiten*, Berichte Sachische Academie der Wissenschaften, Leipzig, Math-Phys. K1 **69** (1917), 262-267.

[8] Salzberg, P., and M. Figueroa "Tomography on the 3D-Torus and Crystals", Chapter 19, Discrete Tomography: Foundations, Algorithms and Applications, Eds G. Herman, A. Kuba, Birkhauser, Boston, 1999.

[9] Svalbe, I., *Natural Representations for the Hough Transform*, IEEE T-PAMI **12**(2) (1991), 336-342.

[10] Svalbe, I., *A Method to Embed Messages in Images Using the Digital Radon Transform*, accepted for presentation at ICIP, Thessalonika, October, 2001.

[11] Svalbe, I., D. van der Spek, *Tomography and the Discrete Radon Transform*, Workshop on Discrete Tomography, Siena, Italy, October, 2000 (submitted to Linear Algebra).

[12] Svalbe, I., *Image Operations in Radon Space*, submitted to DICTA 2002, Melbourne, Australia, Jan 21-22, 2002.

[13] Schroeder, R. M., "Number Theory in Science and Communications", 2nd Edn, Springer-Verlag, 1997.